SCIENCE CHINA
Earth Sciences

•RESEARCH PAPER•

April 2019 Vol.62 No.4: 703–718
https://doi.org/10.1007/s11430-018-9308-9

Evaluation of the SMOS and SMAP soil moisture products under different vegetation types against two sparse *in situ* networks over arid mountainous watersheds, Northwest China

Lanhui ZHANG[1], Chansheng HE[1,2*], Mingmin ZHANG[1] & Yi ZHU[1]

[1] *Key Laboratory of West China's Environmental System (Ministry of Education), College of Earth and Environmental Sciences, Lanzhou University, Lanzhou 730000, China;*
[2] *Department of Geography, Western Michigan University, Kalamazoo, Michigan 49008, USA*

Received May 31, 2018; revised October 8, 2018; accepted November 23, 2018; published online February 12, 2019

Abstract Assessment of the suitability of satellite soil moisture products at large scales is urgently needed for numerous climatic and hydrological researches, particularly in arid mountainous watersheds where soil moisture plays a key role in land-atmosphere exchanges. This study presents evaluation of the SMOS (L2) and SMAP (L2_P_E and L2_P) products against ground-based observations from the Upstream of the Heihe River Watershed *in situ* Soil Moisture Network (UHRWSMN) and the Ecological and Hydrological Wireless Sensor Network (EHWSN) over arid high mountainous watersheds, Northwest China. Results show that all the three products are reliable in catching the temporal trend of the *in situ* observations at both point and watershed scales in the study area. Due to the uncertainty in brightness temperature and the underestimation of effective temperature, the SMOS L2 product and both the SMAP L2 products show "dry bias" in the high, cold mountainous area. Because of the more accurate brightness temperature observations viewing at a constant angle and more suitable estimations of single scattering albedo and optical depth, both the SMAP L2 products performed significantly better than the SMOS product. Moreover, comparing with station density of *in situ* network, station representation is much more important in the evaluation of the satellite soil moisture products. Based on our analysis, we propose the following suggestions for improvement of the SMOS and SMAP product suitability in the mountainous areas: further optimization of effective temperature; revision of the retrieval algorithm of the SMOS mission to reduce the topographic impacts; and, careful selection of *in situ* observation stations for better representation of *in situ* network in future evaluations. All these improvements would lead to better applicability of the SMOS and SMAP products for soil moisture estimation to the high elevation and topographically complex mountainous areas in arid regions.

Keywords SMOS, SMAP, Evaluation, Different vegetation types, Sparse *in situ* networks, Arid mountainous watershed

Citation: Zhang L, He C, Zhang M, Zhu Y. 2019. Evaluation of the SMOS and SMAP soil moisture products under different vegetation types against two sparse *in situ* networks over arid mountainous watersheds, Northwest China. Science China Earth Sciences, 62: 703–718, https://doi.org/10.1007/s11430-018-9308-9

1. Introduction

Soil moisture strongly influences the energy and water cycle in land surface (Koster et al., 2004, 2010; Vereecken et al., 2014; Brooks et al., 2015; Taylor, 2015; Yang et al., 2018). Long-term observations of soil moisture over large areas are critical to numerous climatic and hydrological researches and applications, such as model simulations (Frye and Mote, 2010a, 2010b; Han et al., 2014; Ridler et al., 2014), critical zone hydrology processes (Richter and Mobley, 2009), land-surface interactions (Koster et al., 2004, 2010; Yang et al., 2018), etc. Recently, satellite products of soil moisture have

* Corresponding author (email: He@wmich.edu)

become effective ways to provide surface soil moisture data over large scales. The L-band products are most advantageous because of their strong penetration ability to both soil and vegetation, especially in arid areas where soil moisture is a key factor influencing land-atmosphere exchanges (Kerr et al., 2001; Entekhabi et al., 2010; Zhang et al., 2017a).

Two latest L-band products, Soil Moisture and Ocean Salinity (SMOS) from European Space Agency (ESA), and Soil Moisture Active/Passive (SMAP) from the United States National Aeronautics and Space Administration (NASA), are the most promising satellite soil moisture products (Kerr et al., 2001; Entekhabi et al., 2010). As retrieval based on indirect measurements of satellite products leads to uncertainty, a large number of researches have focused on the evaluation or validation of the satellite soil moisture products. In recent years, the SMOS product has been validated at both global scale (Leroux et al., 2013; Kerr et al., 2016), and regional scale such as the Soil Climate Analysis Network (SCAN)/SNOwpack TELemetry (SNOTEL) network over the continental U.S. (Al Bitar et al., 2012; Jackson et al., 2012), Soil Moisture Observing System-Meteorological Automatic Network Integrated Application (SMOSMANIA) in southwestern France (Parrens et al., 2012), Maqu in China and Twente in the Netherland (Dente et al., 2012), the central Tibetan Plateau in China (Zhao et al., 2014; Li et al., 2018), Duero Basin in Spain (González-Zamora et al., 2015), Saskatchewan in Canada (Djamai et al., 2015), and Iberian Peninsula in southwest Europe (Polcher et al., 2016), etc. In contrast, as the latest mission with a short operation period, the SMAP products have mainly been evaluated at the Core Validation Sites (CVS) (Vreugdenhil et al., 2013; Reichle et al., 2014; O'Neill et al., 2016; Pan et al., 2016; Al-Yaari et al., 2017; Colliander et al., 2017a, 2017b; Ma et al., 2017), with only a few researches being conducted over other regions (Zhang et al., 2017a; Li et al., 2018).

In mountainous areas, the brightness temperature simulations are significantly affected by the surrounding reflection, and it is difficult to solely derive the viewing angles of incidence from the radiometer observation angle in the target area (Pellarin et al., 2016), which makes the retrieval of soil moisture much more difficult and uncertain. Due to the constraints of both accessibility and data availability, little has been reported on the evaluation of the SMOS and SMAP products in mountainous areas (Kang et al., 2017). To our knowledge, only three researches have compared the performance of the SMOS and SMAP products in five CVS and SCAN, Genhe area of Northern China, and a forested area of Northeast China, respectively, none is in high mountainous area (Chen et al., 2017; Cui et al., 2017; Jin et al., 2017).

Therefore, this study aims to evaluate and compare the reliability of the SMOS and SMAP products in the upstream of the Heihe River Watershed, Northwest China. First, we evaluate the SMOS and SMAP products against two sparse *in situ* networks, the Upstream of the Heihe River Watershed *in situ* Soil Moisture Network (UHRWSMN) and the Ecological and Hydrological Wireless Sensor Network (EHWSN). Subsequently, based on the evaluation results, we analyze the suitability of both the SMOS and SMAP products in high mountainous area. Finally, we propose future improvements to both SMOS and SMAP products for estimation of the soil moisture over the high elevation, mountainous areas.

2. Data and methods

2.1 *In situ* measurements

The upstream of the Heihe River Watershed is located in the Qilian Mountain ranges (Figure 1). The length is 313 km and the drainage area is approximately 10009 km^2. With complex terrain surface, the range of the elevation in the upstream is from 1674 to 5584 m asl (meter above sea level) (Li et al., 2009; Zhang et al., 2017b), and the major vegetation types include coniferous forest, shrub, steppe, alpine meadow, alpine sparse vegetation, and barren land (Gao et al., 2016). With an area of 2495 km^2, the Babaohe River Watershed is the eastern branch of the upstream of the Heihe River Watershed (Figure 1). The elevation ranges from 2629 to 4897 m asl with an average value of 3604 m asl. Grassland is the most dominant land-cover types, accounting for 43.94% of the Babaohe River Watershed (Lei et al., 2014).

Due to its high elevation, and complex topography, it is difficult to obtain soil moisture data at watershed scale in the upstream of the Heihe River Watershed (Kang et al., 2017). In the study area, there are limited *in situ* observations only available from the two sparse networks, the UHRWSMN over the upstream of the Heihe River Watershed and the EHWSN over the Babaohe River Watershed. Sparse network measurements are important auxiliary resources for the validation of satellite soil moisture products over large scales (Chen et al., 2017; Colliander et al., 2017a). In this study, all the *in situ* observations from two sparse networks are used to evaluate both the SMOS and SMAP products.

The UHRWSMN was established in June 2013 by authors' team. It includes 35 nodes, installed on the main soil-vegetation combinations in the study area (Figure 1; Table 1). Soil moisture has been measured at depths of 5, 15, 25, 40 and 60 cm with 30-minute intervals by Decagon's 5TE for each node. In this study, the data at 5 cm depths were used as the surface data for evaluation. As part of the Hiwater (Heihe Watershed Allied Telemetry Experimental Research) project (Li et al., 2013), the EHWSN was established in July 2013 in the Babaohe River Watershed (Kang et al., 2017). It includes 40 nodes, which were all installed on grassland at an average distance of 10 km and at an average altitude of 3581 m asl

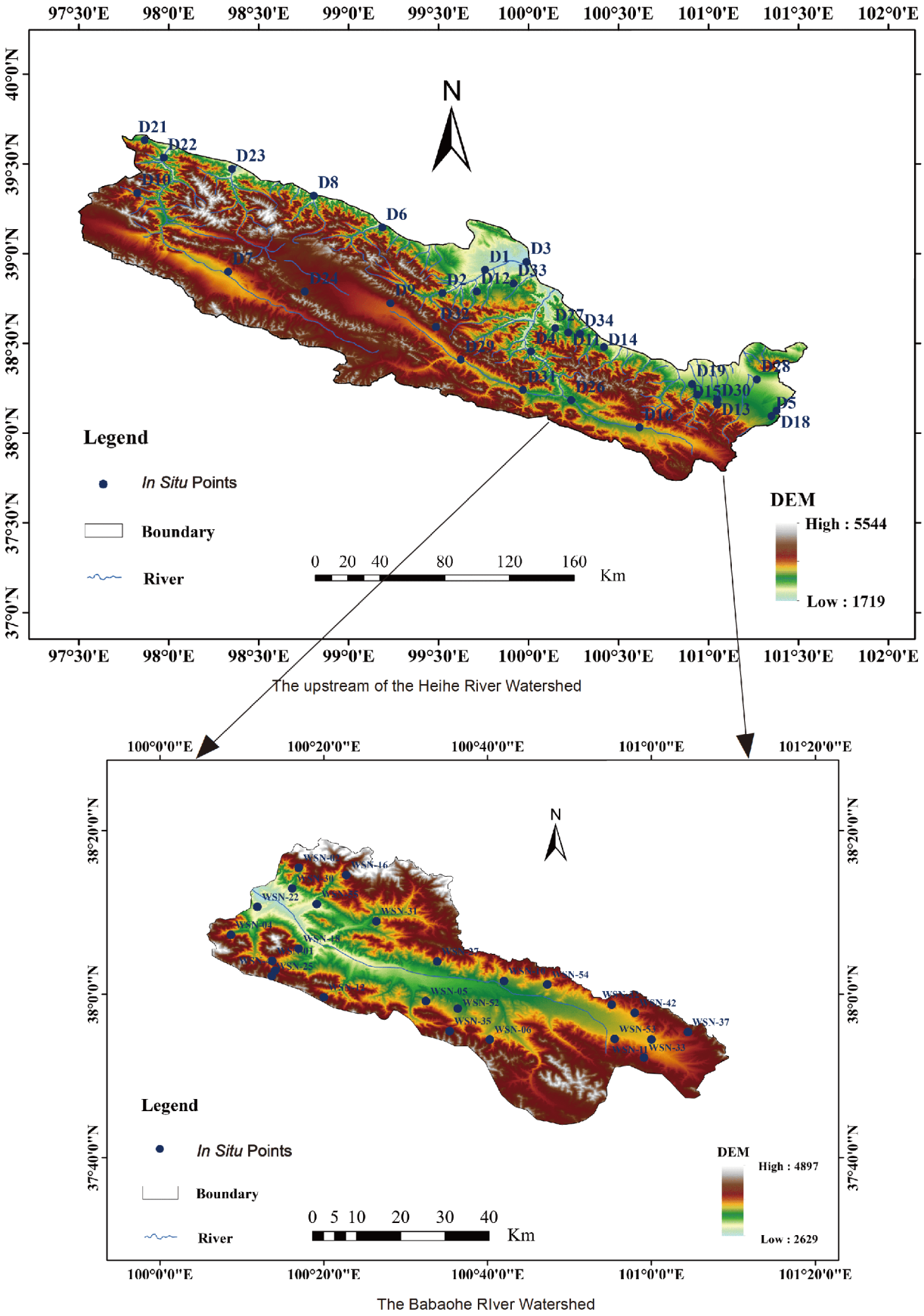

Figure 1 The study area.

Table 1 The UHRWSMN over the upper reach of the Heihe River Watershed

Station	Logitude	Latitude	Altitude (m asl)	Vegetation	Sand (%)	Silt (%)	Clay (%)	Soil types
D1	99.758°E	38.910°N	2151	Sparse grassland	33.890	58.970	7.140	Typical Sierozems
D2	99.520°E	38.781°N	2556	Sparse grassland	32.330	60.020	7.650	Light Castanozems
D3	99.988°E	38.955°N	1827	Sparse grassland	38.030	55.880	6.090	Clay gray desert soils
D4	100.013°E	38.455°N	2370	Sparse grassland	27.819	65.997	6.184	Typical Castanozems
D5	101.350°E	38.095°N	2558	Dense grassland	57.845	37.866	4.289	Light Castanozems
D6	99.186°E	39.146°N	2604	Sparse grassland	25.207	66.891	7.902	Light Castanozems
D7	98.329°E	38.899°N	3317	Sparse grassland	22.072	69.032	8.896	Calcareous Frigid frozen soils
D8	98.805°E	39.323°N	2170	Sparse grassland	20.128	72.581	7.291	Saturated Frigid frozen felt soils
D9	99.232°E	38.724°N	3622	Dense grassland	34.464	58.182	7.354	Saturated Frigid frozen felt soils
D10	97.824°E	39.338°N	3117	Sparse grassland	9.774	82.888	7.337	Calcareous Frigid frozen soils
D11	100.220°E	38.560°N	2890	Coniferous forest	11.134	81.961	6.905	Typical Castanozems
D12	99.711°E	38.789°N	2498	Coniferous forest	19.863	73.599	6.538	Typical Grey-cinnamon soils
D13	101.048°E	38.189°N	2977	Shrub	13.816	78.380	7.804	Peat Frigid felt soils
D14	100.418°E	38.480°N	2676	Coniferous forest	44.335	50.187	5.478	Light Castanozems
D15	101.050°E	38.160°N	3146	Shrub	9.022	83.357	7.621	Peat Frigid felt soils
D16	100.616°E	38.031°N	3105	Dense grassland	28.634	65.963	5.403	Saturated Frigid frozen felt soils
D17	100.929°E	38.065°N	3300	Sparse grassland	25.191	67.730	7.079	Typical Chernozems
D18	101.378°E	38.125°N	2787	Dense grassland	27.410	65.161	7.429	Dry farming Chernozems
D19	100.908°E	38.274°N	2697	Cropland	14.628	78.103	7.268	Typical Castanozems
D20	99.670°E	39.119°N	2147	Barren land	20.753	71.602	7.644	Calcareous Frigid calcic soils
D21	97.866°E	39.633°N	2770	Sparse grassland	25.212	68.056	6.732	Calcareous Frigid calcic soils
D22	97.971°E	39.535°N	2303	Sparse grassland	27.226	66.467	6.307	Saturated Frigid frozen felt soils
D23	98.351°E	39.472°N	2390	Sparse grassland	41.253	53.508	5.239	Typical Frigid frozen calcic soils
D24	98.756°E	38.788°N	4109	Barren land	41.699	52.654	5.648	Typical Frigid desert soils
D25	99.475°E	38.611°N	4155	Barren land	54.860	40.260	4.880	Saturated Frigid frozen felt soils
D26	100.237°E	38.184°N	3252	Sparse grassland	29.832	61.556	8.612	Typical Castanozems
D27	100.147°E	38.585°N	2465	Dense grassland	8.744	81.255	10.002	Light Castanozems
D28	101.269°E	38.299°N	2601	Dense grassland	14.337	73.138	12.524	Typical Castanozems
D29	99.623°E	38.409°N	3249	Dense grassland	22.241	69.842	7.917	Peat Frigid felt soils
D30	101.050°E	38.165°N	3109	Dense grassland	20.356	73.725	5.920	Saturated Frigid frozen felt soils
D31	99.969°E	38.241°N	2920	Dense grassland	24.748	69.119	6.133	Saturated Frigid frozen felt soils
D32	99.485°E	38.592°N	3800	Alpine meadow	26.737	63.807	9.455	Typical Gray calcic soils
D33	100.286°E	38.554°N	2698	Dense grassland	19.860	73.600	6.540	Typical Castanozems
D34	100.937°E	38.215°N	2886	Dense grassland	9.480	84.390	6.130	Typical Chernozems
D35	99.915°E	38.833°N	2839	Dense grassland	27.930	67.160	4.910	Typical Castanozems

(Figure 1; Table 2). For each node, soil moisture has been observed at depths of 4, 10 and 20 cm with 5-minute intervals by soil moisture sensor (Steven's Hydra) in the Babaohe River Watershed. The data at 4 cm depths were used as the surface data for evaluation in this study. Because of instrument malfunctions, ground observations from only 25 of the 40 nodes were available in 2015 to evaluate both the SMOS and SMAP products (Figure 1). The soil moisture data from the EHWSN were downloaded from Environmental & Ecological Science Data Center for West China, National Natural Science Foundation of China (http://westdc.westgis.ac.cn). As the UHRWSMN and EHWSN have been observed on the main vegetation-soil combinations, both of them are comparable with dense *in situ* networks (Kerr et al., 2016; Zhang et al., 2017a).

2.2 Satellite products

The ESA's SMOS mission was launched on November 2009, aiming to provide surface soil moisture (usually the top 5 cm) data at a spatial resolution better than 50 km, with a target accuracy of 0.04 m^3 m^{-3} overland (Kerr et al., 2001).

Table 2 The EHWSN in the Babaohe River Watershed

In situ points	Logitude	Latitude	Altitude (m asl)
WSN-54	100.788°E	38.020°N	3484
WSN-11	101.000°E	37.908°N	3449
WSN-16	100.379°E	38.243°N	3766
WSN-31	100.440°E	38.149°N	3462
WSN-35	100.589°E	37.925°N	3767
WSN-18	100.282°E	38.093°N	3792
WSN-04	100.144°E	38.121°N	3458
WSN-01	100.228°E	38.068°N	3538
WSN-53	100.925°E	37.909°N	3526
WSN-12	100.333°E	37.994°N	3813
WSN-55	100.319°E	38.184°N	3045
WSN-27	100.564°E	38.067°N	3414
WSN-30	100.269°E	38.216°N	3091
WSN-40	100.234°E	38.048°N	3656
WSN-32	100.919°E	37.979°N	3580
WSN-52	100.606°E	37.971°N	3335
WSN-05	100.541°E	37.986°N	3356
WSN-02	100.282°E	38.258°N	3818
WSN-22	100.198°E	38.178°N	3050
WSN-37	101.074°E	37.923°N	3744
WSN-25	100.227°E	38.037°N	3846
WSN-06	100.671°E	37.908°N	3635
WSN-42	100.966°E	37.962°N	3515
WSN-33	100.985°E	37.871°N	3661
WSN-10	100.700°E	38.027°N	3478

The SMOS L2 v.6.2.0 soil moisture data from 1 April 2015 to 22 June 2017 were selected for this research. The data affected by Radio Frequency Interferences (RFI) or with Data Quality Index (DQX) greater than 0.06 were discarded. In the study area, the SMOS L2 product is with a resolution of about 15 km by 15 km, and the equal grids are known as the Discrete Global Grid (DGG) (González-Zamora et al., 2015). The upstream of the Heihe River Watershed is covered by roughly 95 DGGs of the SMOS L2 product, while the Babaohe River Watershed is covered by roughly 16 DGGs (Please see http://www.esa.int/Our_Activities/Observing_the_Earth/SMOS for detailed information).

The NASA's SMAP mission, launched in 2015, was designed to provide global mapping of surface soil moisture (the top 5 cm) with ubRMSE (unbiased root-mean-square errors) less than 0.04 m^3 m^{-3} for the gridded products (36 and 9 km) within the retrieval domain (Entekhabi et al., 2010, 2014; O'Neill et al., 2016). Among the SMAP products at four levels, the Level 2 (L2) products are geophysical retrievals (Entekhabi et al., 2014; Colliander et al., 2017a). The SMAP L2_P product is the retrieval from brightness temperature with a grid cell of 36 km by 36 km. Given that the SMAP radar failed in July 2015, the SMAP L2_P_E product with a resolution of 9 km by 9 km is the soil moisture retrieval from downloaded brightness temperature with original resolution of 36 km by 36 km. Thus, both the SMAP L2_P and the SMAP L2_P_E from 1 April 2015 to 22 June 2017 over the study area were selected for validation in this research. The upstream of the Heihe River Watershed is covered by roughly 32 DGGs of the SMAP L2 product, while the Babaohe River Watershed is covered by roughly 6 DGGs. As to the SMAP L2_P_E product, the upstream of the Heihe River Watershed is covered by roughly 337 DGGs, while the Babaohe River Watershed is covered by roughly 43 DGGs. Both the SMAP L2_P and L2_P_E products are distributed by NASA National Snow and Ice Data Center Distributed Active Archive Center (NSIDC DAAC) and the NASA Alaska Satellite Facility Distributed Active Archive Center (ASF DAAC) (For the SMAP data and further details, please visit http://nsidc.org/).

2.3 Evaluation methods

In order to compare with other evaluation results, four me-

trics: correlation coefficient (R), root-mean-square errors (RMSE), the mean bias (bias) and ubRMSE, were applied to validate all the three products in this study (Brown et al., 2013; Entekhabi et al., 2014; Al-Yaari et al., 2014; Wu et al., 2016; Zhang et al., 2017a).

$$R = \frac{\sum_{t=1}^{n}(\mathrm{SM}_t^{\mathrm{obs}} - \overline{\mathrm{SM}}^{\mathrm{obs}})(\mathrm{SM}_t^{\mathrm{sat}} - \overline{\mathrm{SM}}^{\mathrm{sat}})}{\sqrt{\sum_{t=1}^{n}(\mathrm{SM}_t^{\mathrm{obs}} - \overline{\mathrm{SM}}^{\mathrm{obs}})^2}\sqrt{\sum_{i=1}^{n}(\mathrm{SM}_t^{\mathrm{sat}} - \overline{\mathrm{SM}}^{\mathrm{sat}})^2}}, \quad (1)$$

$$\mathrm{RMSE} = \sqrt{\frac{\sum_{t=1}^{n}(\mathrm{SM}_t^{\mathrm{obs}} - \mathrm{SM}_t^{\mathrm{sat}})^2}{n}}, \quad (2)$$

$$\mathrm{bias} = \overline{\mathrm{SM}}^{\mathrm{sat}} - \overline{\mathrm{SM}}^{\mathrm{obs}}, \quad (3)$$

$$\mathrm{ubRMSE}^2 = \mathrm{RMSE}^2 - \mathrm{bias}^2, \quad (4)$$

where $\mathrm{SM}_t^{\mathrm{obs}}$ is the *in situ* soil moisture on tth day, and $\mathrm{SM}_t^{\mathrm{sat}}$ is the soil moisture of satellite products on tth day. $\overline{\mathrm{SM}}^{\mathrm{obs}}$ and $\overline{\mathrm{SM}}^{\mathrm{sat}}$ are the average values of $\mathrm{SM}_t^{\mathrm{obs}}$ and $\mathrm{SM}_t^{\mathrm{sat}}$ during the entire evaluation period, and n is the total number of days of the evaluation period. R ranges in [−1, 1], the larger values mean that the products better match the observation. RMSE and bias can be any value, while ubRMSE are positive values, the smaller values of these three indices indicate that the products fit the observations better.

2.4 Temporal stability analysis

The temporal stability analysis has also been conducted in this study because it reflects the tempo-spatial distribution of soil moisture with little dependence on the absolute values of soil moisture and less influence of the sampling size (Rötzer et al., 2014). For each grid x, the stability of soil moisture estimates from one time step to another is evaluated by mean relative difference (MRD) $\overline{\delta x}$ and standard deviation $\sigma(\delta_x)$ (Polcher et al., 2016; Zhang et al., 2017a).

$$\overline{\delta_x} = \frac{1}{n}\sum_{t=1}^{n}\delta_{xt}, \quad (5)$$

$$\sigma(\delta_x) = \sqrt{\frac{1}{n-1}\sum_{t=1}^{n}(\delta_{xt} - \overline{\delta x})^2}, \quad (6)$$

where n is the number of days during the evaluation period, δ_{xt} is the relative difference of grid x at tth day, and $\overline{\delta_x}$ is the average value of δ_{xt} of grid x during the evaluation period.

$$\delta_{xt} = \frac{\mathrm{SM}_{xt}^{\mathrm{sat}} - \overline{\mathrm{SM}}_t^{\mathrm{sat}}}{\overline{\mathrm{SM}}_t^{\mathrm{sat}}}, \quad (7)$$

and $\overline{\mathrm{SM}}_t^{\mathrm{sat}}$ is the areal mean value for all m grids at tth day and calculated as eq. (8),

$$\overline{\mathrm{SM}}_t^{\mathrm{sat}} = \frac{1}{m}\sum_{x=1}^{m}\mathrm{SM}_{xt}^{\mathrm{sat}}, \quad (8)$$

and $\mathrm{SM}_{xt}^{\mathrm{sat}}$ is the soil moisture estimates of the SMOS product and both the SMAP products for grid x at tth day. Generally, drier (wetter) areas will get a low (high) MRD and with a low (high) rank, and higher standard deviations of MRDs indicate a lower persistence of soil moisture distribution over time (Rötzer et al., 2014). The similarity of MRD ranks measures the spatial distribution similarity of different products, while the standard deviations of MRD indicate the persistence of soil moisture distribution over time, i.s. the smaller the $\sigma(\delta_x)$, the greater persistence of the soil moisture distribution over time.

3. Results

3.1 Evaluation of the SMOS and SMAP products of overpassing orbits

As the ascending and descending retrievals of both the SMOS and SMAP products show different performance (Entekhabi et al., 2014; Zhao et al., 2014), both ascending and descending overpasses of each product were investigated in this study. The SMOS and SMAP products of each overpassing orbit were compared with the corresponding observations from UHRWSMN (2015-04-01–2017-07-22) over the upstream of the Heihe River Watershed, and from EHWSN (2015-04-01–2015-12-31) over the Babaohe River Watershed. As shown in Table 3, the R values are 0.367–0.608, all passing significance test of 0.001, indicating that all the three products of both the ascending and descending orbits performed well in catching the trend of the observations. All the bias values are negative, thus the SMOS L2 product and both the SMAP L2 products showed "dry bias" with underestimation of the soil moisture (Rötzer et al., 2014; Zhang et al., 2017a). With the RMSE values ranging from 0.063 to 0.161 $\mathrm{m^3\ m^{-3}}$ and the ubRMSE values ranging from 0.056 to 0.118 $\mathrm{m^3\ m^{-3}}$, all being evaluated at the point scale, all the three products did not achieve the target accuracy of 0.04 $\mathrm{m^3\ m^{-3}}$.

Furthermore, as shown in Table 3, in both watersheds, both the SMAP L2 products showed similar performance with slightly smaller R values, smaller RMSE and ubRMSE values of the SMAP L2_P product, and both of them performed notably better than the SMOS L2 product with significantly larger R values, smaller *RMSE* and ubRMSE values.

3.2 Evaluation of the SMOS and SMAP Products at the watershed scale

Due to its complex topography, accurate estimation of soil moisture at the watershed scale in the study area is very difficult in the Heihe River Watershed (Kang et al., 2017). For fair comparison, the SMOS L2 product, the SMAP L2_P and L2_P_E products, and *in situ* observations were all processed into daily areal average values in both watersheds

Table 3 Evaluation of the SMOS and both SMAP products in the study area

In situ networks	Product	Overpassing moments	*R*	RMSE ($m^3\ m^{-3}$)	Bias ($m^3\ m^{-3}$)	ubRMSE ($m^3\ m^{-3}$)	*n*
UHRWSMN	The SMOS Product	Asc	0.390*	0.094	−0.020	0.091	1838
		Des	0.519*	0.093	−0.027	0.090	3016
	The SMAP L2_P_ E Product (9 km)	Asc	0.554*	0.065	−0.033	0.056	7073
		Des	0.607*	0.063	−0.027	0.056	6397
	The SMAP L2_P Product (36 km)	Asc	0.565*	0.066	−0.030	0.059	6660
		Des	0.608*	0.064	−0.023	0.060	5961
EHWSN	The SMOS Product	Asc	0.367*	0.144	−0.092	0.111	497
		Des	0.391*	0.161	−0.109	0.118	1016
	The SMAP L2_P_ E Product (9 km)	Asc	0.442*	0.132	−0.103	0.083	1699
		Des	0.441*	0.134	−0.107	0.080	1526
	The SMAP L2_P Product (36 km)	Asc	0.464*	0.139	−0.110	0.086	1638
		Des	0.450*	0.141	−0.115	0.082	1443

a) * Refers to passing significance test of 0.001. ASC refers to ascending, Des refers to descending.

at the watershed scale (Figure 2). For the SMOS L2, SMAP L2_P and L2_P_E products, the *R* values are 0.584, 0.737 and 0.803 respectively in the upstream of the Heihe River Watershed, while they are 0.597, 0.490 and 0.611 respectively in the Babaohe River Watershed. It indicates that all the three products performed very well in capturing soil moisture dynamics in both watersheds. The ubRMSE values are 0.050, 0.031 and 0.027 $m^3\ m^{-3}$ for the SMOS L2, SMAP L2_P and L2_P_E products respectively in the upstream of the Heihe River Watershed, while they are 0.062, 0.039 and 0.039 $m^3\ m^{-3}$ respectively in the Babaohe River Watershed. Thus at the watershed scale, the SMOS L2 product did not achieve the target accuracy of 0.04 $m^3\ m^{-3}$, while both the SMAP L2 products are far beyond the target accuracy in both watersheds. All the three products also show "dry bias" at the watershed scale with all negative bias values in both watersheds. It is worth mentioning that, all the SMOS L2, SMAP L2_P and L2_P_E products lacked data in winter (from December to March) in the study area (Figure 2).

Because of limited data availability, the ubRMSE values are used as the main index to compare performance of all the three products (Zhang et al., 2017a). In both watersheds, the SMAP L2_P_E performed better than the L2_P product, and both of them performed significantly better than the SMOS L2 product.

3.3 Evaluation of the SMOS and SMAP Products under different vegetation types

For L-band products, only less than 0.7% of the volumetric error is caused by soil heterogeneity (Galantowicz et al., 2000). As shown in Table 1, there is little difference in soil textures of the *in situ* nodes in this study. Vegetation is the most important factor influencing the retrieval accuracy of satellite soil moisture products at both global and regional scales (Galantowicz et al., 2000; Wigneron et al., 2012; Leroux et al., 2013; Djamai et al., 2015). Thus, the SMOS and both SMAP products have been compared with the time series of *in situ* soil moisture under different vegetation types (Table 4). In the upstream of the Heihe River Watershed, the performance of both the SMAP L2 products shows a declining order of cropland, coniferous forest, dense grassland and sparse grassland, alpine meadow, and shrub. The SMOS L2 product performed best under coniferous forest and cropland, then sparse grassland, dense grassland, and finally alpine meadow and shrub. Both the SMAP L2_P and L2_P_E products achieved the target accuracy of 0.04 $m^3\ m^{-3}$ for all the vegetation types except alpine meadow and shrub, while the SMOS L2 product did not achieve the target accuracy under all the vegetation types.

In the upstream of the Heihe River Watershed, both the SMAP L2_P and L2_P_E products showed significantly better performance than the SMOS L2 product under all the vegetation types. In the Babaohe River Watershed, as all the *in situ* observation sites were on grassland, the better performance of two SMAP L2 products indicates that both of them performed better than the SMOS L2 product under the grasslands (Table 4). Therefore, both the SMAP L2 products performed significantly better than the SMOS L2 product under all the vegetation types in both watersheds.

3.4 Performance comparison of the three products in UHRWSMN and EHWSN

To assess the impacts of *in situ* observation station density on the validation of the SMOS and SMAP soil moisture products in the study area, all the three products were evaluated against both UHRWSMN and EHWSN during the same period from 2015-04-01 to 2015-12-31. As shown in Table 5, although with slightly smaller *R* values of ascending overpass in UHRWSMN, the significantly smaller RMSE, absolute bias, and ubRMSE values indicate that the SMOS

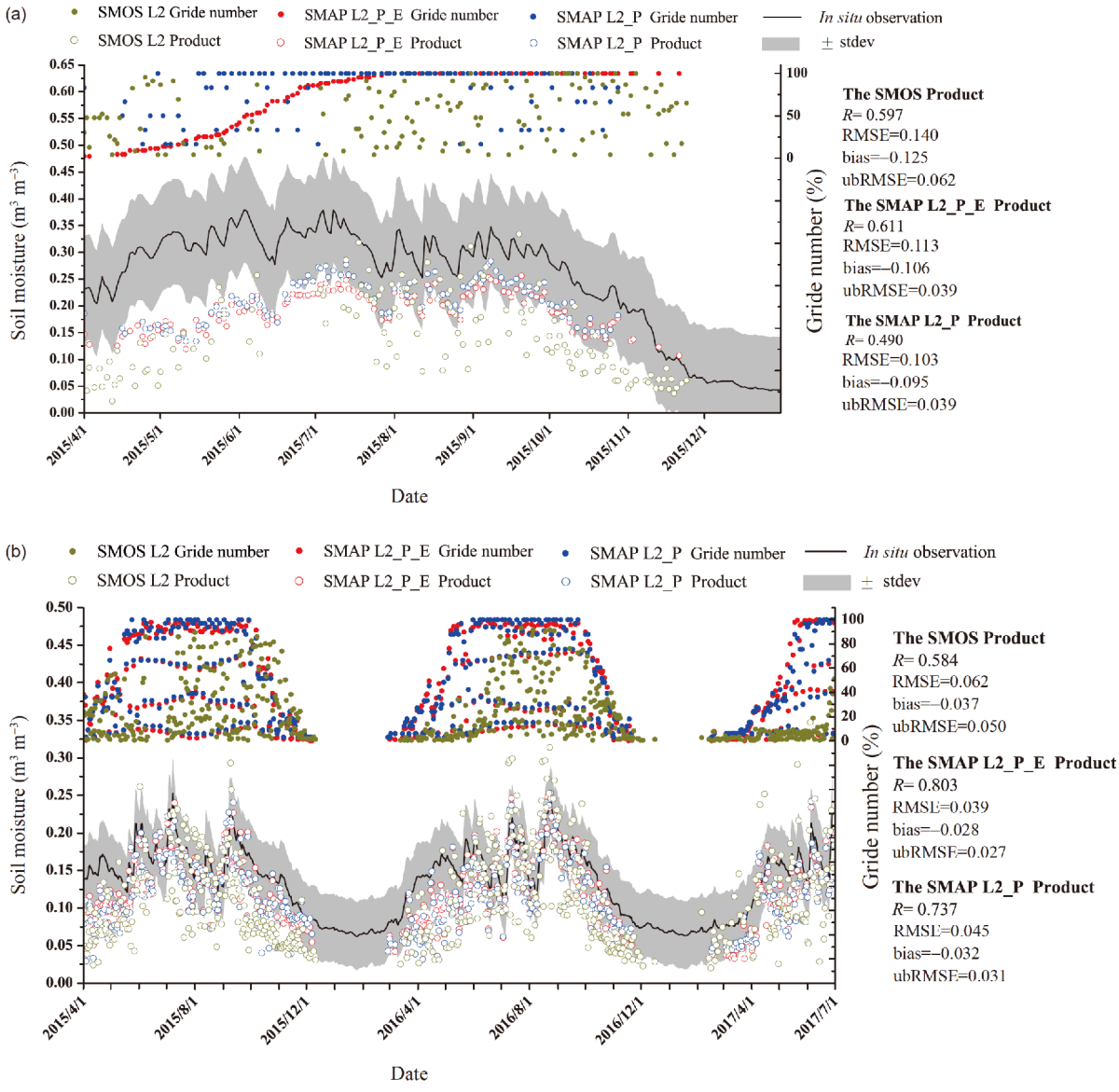

Figure 2 Time series of daily areal average values of the SMOS, both the SMAP products and *in situ* observations. (a) The upper reach of the Heihe River Watershed; (b) the Babaohe River Watershed.

product performed better in UHRWSMN than EHWSN of ascending overpass. For descending overpass, the SMOS product also performed better in UHRWSMN than EHWSN with larger R values, smaller RMSE, absolute bias, and ubRMSE values. Similarly, with larger R values, smaller RMSE, absolute bias, and ubRMSE values, both the SMAP L2_P_E and L2_P products performed better in UHRWSMN than EHWSN of both ascending and descending overpasses. Thus, both the SMOS and SMAP product performed better in UHRWSMN than EHWSN.

3.5 Temporal stability analysis

Because there were only few grids in the Babaohe River Watershed, the MRDs and their standard deviations of the SMOS L2 product and both the SMAP L2 products were only compared in the upstream of the Heihe River Watershed. As shown in Figure 3, the MRDs are –0.514, –0.561 for the SMOS L2 product, –0.440, –0.999 for the SMAP L2_P product, and –0.491, –0.856 for the SMAP L2_P_E product. The MRD trends of all the three products are smaller in the northwest and larger in the southeast. It means that the soil moisture estimates of the three products are all drier in the northwest and wetter in the southeast of the study area.

The standard deviations of MRDs are 0.225–0.656 with a areal mean value of 0.403 for the SMOS L2 products, and are 0.104, –0.351 with areal mean value of 0.203 for the SMAP L2_P product, and 0.090 to 0.738 with areal mean value of 0.182 for the SMAP L2_P_E product. For all the three products, the standard deviations of MRDs are smaller in the

Table 4 Evaluation of the SMOS and both SMAP products under different vegetation types over the upper reach of the Heihe River Watershed

Product	Vegetation types	R	RMSE ($m^3\ m^{-3}$)	Bias ($m^3\ m^{-3}$)	ubRMSE ($m^3\ m^{-3}$)	n
The SMOS Product	Alpine meadow	0.606*	0.107	−0.055	0.092	137
	Sparse grassland	0.488*	0.075	0.008	0.070	1349
	Dense grassland	0.448*	0.095	−0.031	0.081	1662
	Shrub	0.499*	0.179	−0.156	0.089	275
	Coniferous forest	0.463*	0.072	−0.031	0.064	416
	Cropland	0.543*	0.085	−0.049	0.069	137
	Barren land	0.642*	0.101	0.016	0.082	237
The SMAP L2_P_E Product (9 km)	Alpine meadow	0.751*	0.150	−0.140	0.052	184
	Sparse grassland	0.598*	0.045	0.000	0.035	2261
	Dense grassland	0.575*	0.054	−0.023	0.034	2594
	Shrub	0.163*	0.207	−0.192	0.077	385
	Coniferous forest	0.665*	0.051	−0.038	0.032	743
	Cropland	0.728*	0.067	−0.062	0.026	238
	Barren land	0.633*	0.068	−0.007	0.033	332
The SMAP L2_P Product (36 km)	Alpine meadow	0.727*	0.140	−0.132	0.048	151
	Sparse grassland	0.597*	0.047	0.006	0.036	2344
	Dense grassland	0.584*	0.058	−0.023	0.034	2314
	Shrub	0.224*	0.188	−0.175	0.068	329
	Coniferous forest	0.647*	0.055	−0.044	0.032	684
	Cropland	0.736*	0.042	−0.034	0.025	193
	Barren land	0.664*	0.077	−0.003	0.030	298

a) * refers to passing significance test of 0.001. The indices are average values of both ascending and descending orbits for each product.

Table 5 Comparison of the SMOS and both SMAP products in UHRWSMN and EHWSN from 2015-04-01 to 2015-12-31[a)]

In situ networks	Product	Overpassing moments	R	RMSE ($m^3\ m^{-3}$)	Bias ($m^3\ m^{-3}$)	ubRMSE ($m^3\ m^{-3}$)	n
UHRWSMN	The SMOS Product	Asc	0.348*	0.085	−0.027	0.080	781
		Des	0.425*	0.086	−0.042	0.076	1409
	The SMAP L2_P_E Product (9 km)	Asc	0.540*	0.061	−0.030	0.053	2845
		Des	0.582*	0.060	−0.025	0.054	2504
	The SMAP L2_P Product (36 km)	Asc	0.531*	0.063	−0.027	0.057	2768
		Des	0.579*	0.061	−0.021	0.057	2431
EHWSN	The SMOS Product	Asc	0.367*	0.144	−0.092	0.111	497
		Des	0.391*	0.161	−0.109	0.118	1016
	The SMAP L2_P_E Product (9 km)	Asc	0.442*	0.132	−0.102	0.083	1699
		Des	0.441*	0.134	−0.107	0.080	1523
	The SMAP L2_P Product (36 km)	Asc	0.464*	0.139	−0.110	0.086	1638
		Des	0.450*	0.141	−0.115	0.082	1443

a) * refers to passing significance test of 0.001. ASC refers to ascending, Des refers to descending.

west and larger in the east, indicating that the soil moisture distributions of all the three products showed lower persistence over time in the east than in the west. The SMAP L2_P_E product, with the finest resolution, presents more details of the spatial distribution with smaller standard deviations of MRDs in the central areas and larger standard deviations of MRDs in the outlying areas. It implies that the soil moisture distributions of the SMAP L2_P_E product showed lower persistence over time in the outlying areas than in the central areas. The standard deviations of the SMAP L2_P show smallest range, then the SMOS L2 product and the SMAP L2_P_E product. It suggests that the soil moisture distributions of the SMAP L2_P product had the greatest persistence over time, followed by the SMOS pro-

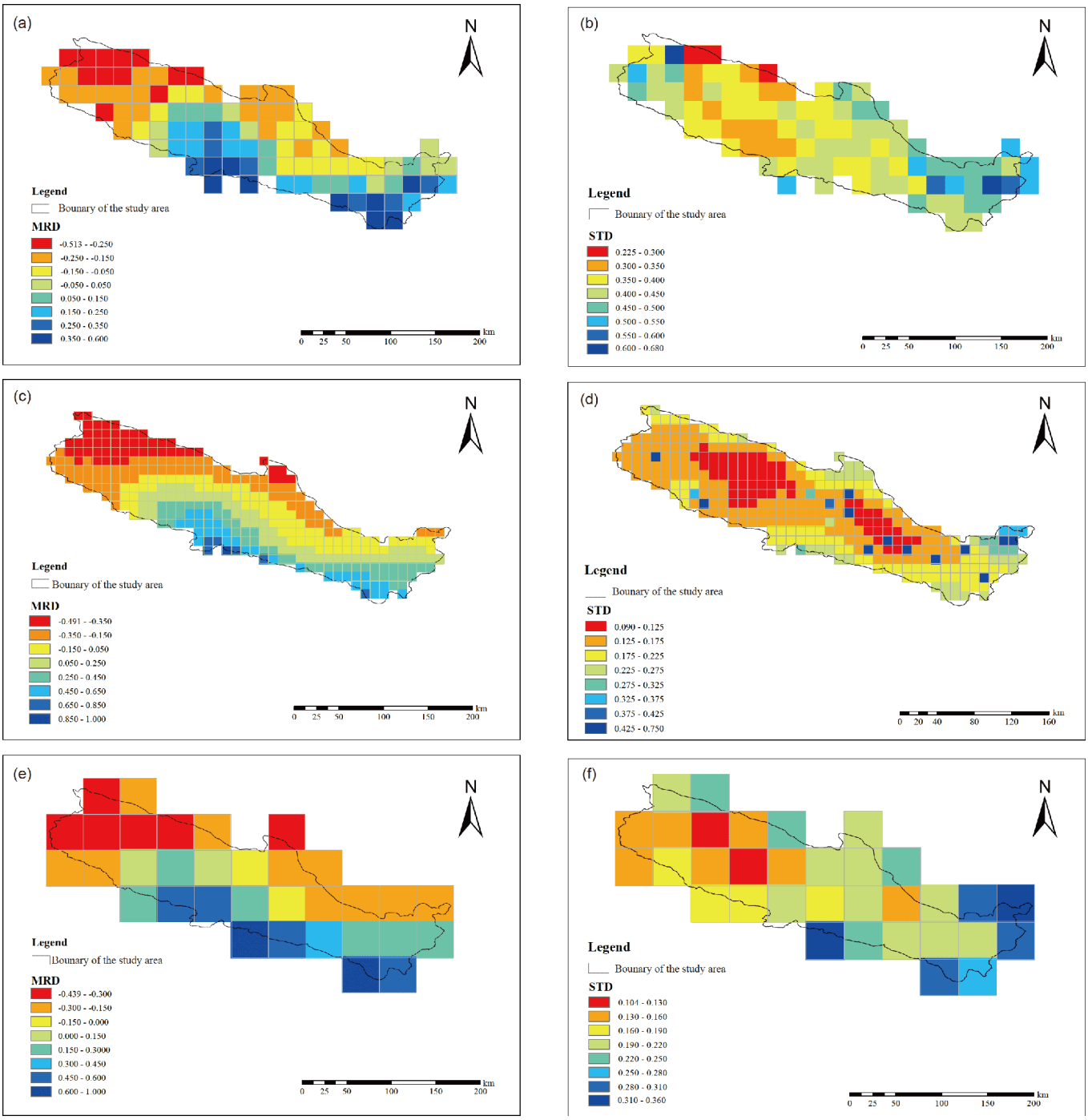

Figure 3 Temporal stability analysis of the SMOS and both SMAP products in the upper reach of the Heihe River Watershed. (a) MRDs of the SMOS product; (b) standard deviation of the SMOS product; (c) MRDs of the SMAP L2_P_E (9 km) product; (d) standard deviation of the SMAP L2_P_E (9 km) product; (e) MRDs of the SMAP L2_P (36 km) product; (f) standard deviation of the SMAP L2_P (36 km) product.

duct and the SMAP L2_P_E product (Figure 3).

4. Discussion

4.1 Impacts of errors in brightness temperature observations and effective temperature estimates

Both the SMOS and SMAP missions are based on the tau-omega model to describe the effects of soil and vegetation on the surface brightness temperature TB_p (Mo et al., 1982; Panciera et al., 2009), which is shown as eq. (9).

$$TB_p(\theta) = (1-\omega_p)(1-\varphi_p(\theta)) (1+\varphi_p(\theta)r_p(\theta))T_v + (1-r_p(\theta))\varphi_p(\theta)T_s, \quad (9)$$

where T_v is the vegetation temperature, T_s is the soil effective temperature, ω_p is the vegetation single scattering albedo,

$\varphi_p(\theta)$ is the vegetation attenuation factor, $r_p(\theta)$ is the soil reflectivity. Both $\varphi_p(\theta)$ and $r_p(\theta)$ generally vary with the measurement polarization p (horizontal or vertical) and the sensor observation angle θ. At L-band, the value of the single scattering albedo ω_p is generally found to be low (Wigneron et al., 2007), and show low sensitivity to polarization, incidence angle (Owe et al., 2001).

To retrieve soil moisture, both missions isolate the soil surface reflectivity $r_p(\theta)$ as eq. (10) by inversion of the tau-omega model:

$$r_p(\theta) = \frac{TB_p(\theta) - (1-\omega_p)(1-\varphi_p(\theta))T_v + \varphi_p(\theta)T_s}{(1-\omega_p)(1-\varphi_p(\theta))\varphi_p(\theta)T_v + \varphi_p(\theta)T_s}. \quad (10)$$

Then, the emissivity $e_p(\theta)$ is related to the soil surface reflectivity by $e_p(\theta)=1-r_p(\theta)$. The Fresnel equation is then used to determine the dielectric constant from the soil emissivity. Finally, a dielectric mixing model is used to solve for the soil moisture given knowledge of the soil texture (Entekhabi et al., 2014; O'Neill et al., 2015; Fernandez-Moran et al., 2017). Thus, the errors of both SMOS and SMAP products are caused by uncertainty in estimating TB_p, T_v, T_s, $\varphi_p(\theta)$ and ω_p.

In this study, the SMOS L2 product, as well as the SMAP L2_P_E and L2_P products, show the "dry bias" at both the point scale and watershed scale in both watersheds. The "dry bias" has also been reported in almost all the validations of both products over mountainous regions (Jackson et al., 2012; Gherboudj et al., 2012; Zhao et al., 2014; Chen et al., 2017; Cui et al., 2017; Ma et al., 2017; Zhang et al., 2017a). In this study, for the SMOS product, because all the *in situ* instruments in EHWSN are installed on the grassland, the performance differences under different vegetation types are only analyzed in UHRWSMN. As shown in Table 4, the SMOS product underestimates soil moisture under all the vegetation types except sparse grassland. As shown in Table 6, the *in situ* observations show stronger variations under driest conditions in sparse grassland, which leads to minor overestimations under sparse grassland. Therefore, the "dry bias" of the SMOS product is not influenced by different vegetation types, indicating that vegetation parameters ω_p and $\varphi_p(\theta)$ in eq. (10) are not main reasons for the "dry bias" of the SMOS product.

Both the SMOS and SMAP missions assume that effective soil (T_s) and vegetation (T_v) temperatures are approximately equal to a single value, effective temperature (T_{eff}) (Kerr et al., 2012b; Srivastava et al., 2013). Zhang et al. (2017a) pointed out that the "dry bias" of the SMAP products was attributed to the uncertainties in estimating the TB_p and T_{eff} in mountainous area. Since the aforementioned analysis indicates that vegetation parameters are not the main reason for the "dry bias" of the SMOS product, it is reasonable to infer that the dry biases of both SMOS and SMAP products are mainly caused by the uncertainties in estimating the brightness temperature TB_p and effective temperature T_{eff} in mountainous area.

In the study area, surface incidence angle of the SMOS product ranges from 31.2° to 45.5°, and surface incidence angle of the SMAP product is a constant of 40°, thus both missions view the targeted landscape at large incidence angles. As the errors of soil moisture retrievals are sensitive to the errors of brightness temperature observations at large incidence angles (Li et al., 2015), the errors in brightness temperature observations would lead to errors in soil moisture retrievals. In mountainous areas, angles of incidence in the target area cannot be derived solely from the radiometer observation angle, and the surrounding reflection significantly affects brightness temperature simulation (Pellarin et al., 2016). Nevertheless, both of them have been ignored in both the SMOS and SMAP missions (Entekhabi et al., 2014). Synthesizing these factors, it is logic to infer that the errors in brightness temperature TB_p is an important cause of the "dry bias".

In both SMOS and SMAP missions, the algorithms to derive soil moisture are very sensitive to the effective temperature T_{eff} (Zhao et al., 2015). If T_{eff} is cooler than the actual temperature, according to eq. (10), it would result in larger estimate of $r_p(\theta)$ and in turn smaller estimate of $e_p(\theta)$, eventually leading to dry retrieval of soil moisture. In the SMOS mission, T_{eff} is estimated by the simulations of the European Centre for Medium-Range Weather Forecasts (ECMWF), but the ECMWF model shows "dry bias" in estimating temperature in China (Ma et al., 2006). In the SMAP mission, T_{eff} is derived from the simulated soil temperature by the Goddard Earth Observing Model System Version 5 (GEOS-5) model (Chen et al., 2017). As shown in Table 7, both the SMAP products significantly underestimated the surface temperatures in both watersheds. Chen et al. (2017) also stated that the underestimation of T_{eff} results in the "dry bias" of the SMAP product in the Tibetan Plateau, which is also a high, cold area close to our study area. Thus, the underestimation of the effective temperature T_{eff} is a main reason for the "dry bias" of both the SMOS and SMAP in mountainous area.

In summary, the "dry bias" of both the SMOS and SMAP products is mainly caused by the uncertainty in brightness temperature TB_p and the underestimation of effective temperature T_{eff} in mountainous area. Such errors in both TB_p and T_{eff} would propagate through the soil moisture inversion algorithm (Das et al., 2016), which is still unclear and requires further investigations in the future.

4.2 Impacts of topography and vegetation conditions

Both the SMAP L2_P and L2_P_E products performed significantly better than the SMOS product at both the point scale and watershed scale in both study watersheds. As shown in Figure 2, most grids lack data from the SMOS L2

Table 6 Statistics of *in-situ* observation under different vegetation types

Statistics (m^3 m^{-3})	Alpine meadow	Sparse grassland	Dense grassland	Shrub	Coniferous forest	Cropland	Barren land
Minimum	0.018	0.002	0.052	0.177	0.048	0.137	0.026
Maximum	0.477	0.370	0.424	0.627	0.294	0.295	0.339
Average	0.295	0.112	0.174	0.355	0.145	0.204	0.151
CV	0.254	0.587	0.311	0.243	0.319	0.143	0.474
Stdev	0.075	0.066	0.054	0.086	0.046	0.029	0.072

Table 7 Evaluation of the surface temperature from both the SMAP products[a)]

In situ networks	Product	Overpassing moments	*R*	RMSE (°C)	Bias (°C)	ubRMSE (°C)	*n*
UHRWSMN	The SMAP L2_P_ E Product (9 km)	Asc	0. 826*	8.399	−7.535	3.710	6885
		Des	0.930*	3.774	−3.072	2.192	6220
	The SMAP L2_P Product (36 km)	Asc	0.796*	8.802	−7.819	4.041	6469
		Des	0.914*	4.038	−3.319	2.301	5774
EHWSN	The SMAP L2_P_ E Product (9 km)	Asc	0.840*	6.517	−5.801	2.970	1703
		Des	0.909*	2.444	−1.935	1.493	1523
	The SMAP L2_P Product (36 km)	Asc	0.829*	6.652	−5.913	3.046	1638
		Des	0.908*	2.285	−1.793	1.417	1443

a) * Refers to passing significance test of 0.001. ASC refers to ascending, Des refers to descending.

product in both watersheds because of strong influence by RFI disturbances (Oliva et al., 2012). This data lacking partially limited the performance of the SMOS L2 product. Other studies have also stated that the SMOS products show worse performance than the SMAP products, due to the different impacts of topography and vegetation on both products (Chen et al., 2017; Cui et al., 2017; Jin et al., 2017).

In the study area, the SMOS mission views the surface at incidence angles ranging from 31.2° to 45.5°, and the SMAP mission views the surface at a constant angle of 40°. The complex terrain surface in the study area may cause changes in the overall surface emissions, and this topographic impact would change with the viewing angle. Because the SMOS mission uses multi-angled measurements to derive soil moisture, it seems to be more influenced by the topography than the SMAP mission (Jin et al., 2017). Other studies also report that the SMOS products show worse performance than the SMAP products in their evaluations, especially in mountainous area (Chen et al., 2017; Cui et al., 2017; Jin et al., 2017). Compared with SMOS, the SMAP mission provides brightness temperature observation with a lower measurement error (De Lannoy et al., 2015). This indicates that topography shows greater impacts on the SMOS product than the SMAP products, leading to worse performance of the SMOS product in mountainous area.

In both the SMOS and SMAP missions, the vegetation attenuation factor $\varphi_p(\theta)$ can be computed from the optical depth $\tau_p(\theta)$ as $\varphi_p(\theta)=\exp(-\tau_p(\theta)/\cos\theta)$. According to eq. (10), the following parameter effects can be distinguished in both missions under vegetation conditions: incident angle θ, vegetation scattering ω_p and optical depth $\tau_p(\theta)$. Although both missions apply the tau-omega model, the SMOS mission and the SMAP mission differ significantly in estimating aforementioned retrieval parameters in eq. (10).

In the SMOS L2 algorithm, the value of ω_p is assumed to be zero over low vegetation canopies (nonforested biomes) and 0.06, –0.08 over forests (Kerr et al., 2012a). In the SMAP L2 algorithm, the values of ω_p are determined in a look-up table ranging from 0.05 to 0.08 for different vegetation types and 0 for barren land (O'Neill et al., 2015; Chan et al., 2016). The ω_p values are 0.02, –0.04 over low vegetation and 0.03, –0.06 over forested areas (Konings et al., 2016), while the optimum ω_p values are 0.08, –0.12 at global scale (Fernandez-Moran et al., 2017). The ω_p values in the SMAP mission are more specific on different vegetation types and closer to the optimum values than in the SMOS mission.

In the SMOS mission, the optical depth $\tau_p(\theta)$ is estimated by $\tau_p(\theta)=\tau_{\mathrm{NAD}}(\theta)(\sin^2(\theta)tt_p+\cos^2(\theta))$. In which, tt_p is the correction parameter for anisotropic effects in the canopy structure, and τ_{NAD} is estimated by the leaf area index (LAT) as $\tau_{\mathrm{NAD}}=b_1\times\mathrm{LAI}+b_2$ (Kerr et al., 2012b). In the SMAP mission, τ_p is estimated by the vegetation water content (VWC) as $\tau_p=b_p\times\mathrm{VWC}$ (Jin et al., 2017). All the vegetation parameters b_1, b_2 and b_p are empirical constants in both missions. Under all the vegetation types, both the SMAP products performed better than the SMOS product in both study watersheds (Table 4). Thus, we can infer that the estimation of $\tau_p(\theta)$ in the SMAP mission is more appropriate than those used in the SMOS mission.

In summary, at a constant view angle, the brightness temperature observations in the SMAP mission are more accurate than the SMOS mission in the study area because of its lower topographic impacts. The estimations of ω_p values and $\tau_p(\theta)$ of the SMAP products are also more suitable in mountainous area. Hence, both the SMAP products performed significantly better than the SMOS product in both watersheds under vegetated surfaces.

4.3 Impacts of station density and representation

Both the SMOS and SMAP products performed better in UHRWSMN than in EHWSN, this is attributable to the station density and representation of *in situ* observations. Generally, higher station density would lead to more accurate evaluation. Because there are two *in situ* stations of UHRWSMN installed on grassland in the Babaohe River Watershed, all the three SMOS and SMAP products have been evaluated by all the stations of both UHRWSMN and EHWSN in the Babaohe River Watershed. As shown in Table 8, evaluated by the combination of four indices, all the three products performed slightly better against all the stations in the Babaohe River Watershed than those only against stations in EHWSN. Because all the *in situ* stations in the Babaohe River Watershed are installed on grassland, the better performance achieved by employing more stations indicates that higher observation station density would show better performance of product evaluation in the study area. In this study, the station density is 35×10^{-4} km^{-2} in UHRWSMN, and 100×10^{-4} km^{-2} in EHWSN. However, even with lower station density, all the SMOS and SMAP products show better performances in UHRWSMN, indicating that station representation is much more important in the evaluation of the satellite soil moisture products.

The soil moisture estimates of all the three products are drier in the northwest and wetter in the southeast of the study area, which is consistent with the precipitation pattern in the study area (Ding et al., 1999; Wang and Zhao, 2013). Partially because of the product resolutions, the soil moisture distributions of both the SMOS L2 and SMAP L2_P products show lower temporal persistence in the east than in the west, while the SMAP L2_P_E product showed lower persistence in the outlying areas than in the central areas. Also because of the product resolution, the soil moisture distributions of the SMAP L2_P product had the greatest persistence over time, followed by the SMOS product and the SMAP L2_P_E product.

5. Conclusion

This study presents evaluation of the SMOS (L2) and SMAP (L2_P_E and L2_P) soil moisture products against two sparse *in situ* networks, the UHRWSMN (2015-04-01–2017-06-22) and EHWSN (2015-04-01–2015-12-31), in the upstream of the Heihe River Watershed, Northwest China. Results show that all the three products performed well in catching the temporal trend of the *in situ* observations in the

Table 8 Comparison of the SMOS product and both SMAP products in UHRWSMN and EHWSN from 2015-04-01 to 2015-12-31[a)]

In situ networks	Product	Overpassing moments	R	RMSE ($m^3\ m^{-3}$)	Bias ($m^3\ m^{-3}$)	ubRMSE ($m^3\ m^{-3}$)	n
UHRWSMN	The SMOS Product	Asc	0.348*	0.085	−0.027	0.080	781
		Des	0.425*	0.086	−0.042	0.076	1409
	The SMAP L2_P_ E Product (9 km)	Asc	0.540*	0.061	−0.030	0.053	2845
		Des	0.582*	0.060	−0.025	0.054	2504
	The SMAP L2_P Product (36 km)	Asc	0.531*	0.063	−0.027	0.057	2768
		Des	0.579*	0.061	−0.021	0.057	2431
EHWSN	The SMOS Product	Asc	0.367*	0.144	−0.092	0.111	497
		Des	0.391*	0.161	−0.109	0.118	1016
	The SMAP L2_P_ E Product (9 km)	Asc	0.442*	0.132	−0.102	0.083	1699
		Des	0.441*	0.134	−0.107	0.080	1523
	The SMAP L2_P Product (36 km)	Asc	0.464*	0.139	−0.110	0.086	1638
		Des	0.450*	0.141	−0.115	0.082	1443
UHRWSMN+ EHWSN in Babaohe River	The SMOS Product	Asc	0.370*	0.139	−0.086	0.110	551
		Des	0.386*	0.155	−0.104	0.115	1119
	The SMAP L2_P_E Product (9 km)	Asc	0.447*	0.125	−0.093	0.083	1884
		Des	0.446*	0.127	−0.097	0.082	1686
	The SMAP L2_P Product (36 km)	Asc	0.471*	0.130	−0.100	0.083	1816
		Des	0.458*	0.132	−0.105	0.080	1596

a) * Refers to passing significance test of 0.001. ASC refers to ascending, Des refers to descending.

study area. Because of the uncertainty in brightness temperature and the underestimation of effective temperature, the SMOS product and both the SMAP products show "dry bias" in high, cold mountainous area.

In the mountainous area, the brightness temperature observations of the SMAP mission are more accurate than the SMOS mission because of its lower topographic impacts at a constant view angle of 40°. The estimations of single scattering albedo ω_p and optical depth $\tau_p(\theta)$ of the SMAP product are also more suitable than the SMOS mission in mountainous area. Thus, both the SMAP products performed significantly better than the SMOS product. Comparing with observation station density of *in situ* network, station representation is much more important in the evaluation of the satellite soil moisture products.

Based on the results of this study, the following suggestions are proposed to improve both the SMOS and SMAP missions in the future: further optimization of effective temperature; revision of the retrieval algorithm of the SMOS mission to reduce the topographic impacts; and careful selection of *in situ* observation stations for better representation of *in situ* network in future evaluations.

Acknowledgements *This work was supported by the National Natural Science Foundation of China (Grant Nos. 41501016, 41530752, and 91125010), the Scherer Endowment Fund of Department of Geography, Western Michigan University and the Fundamental Research Funds for the Central Universities (Grant No. LZUJBKY-2017-224).*

References

Al Bitar A, Leroux D, Kerr Y H, Merlin O, Richaume P, Sahoo A, Wood E F. 2012. Evaluation of SMOS soil moisture products over continental U.S. using the SCAN/SNOTEL network. IEEE Trans Geosci Remote Sens, 50: 1572–1586

Al-Yaari A, Wigneron J P, Ducharne A, Kerr Y, de Rosnay P, de Jeu R, Govind A, Al Bitar A, Albergel C, Muñoz-Sabater J, Richaume P, Mialon A. 2014. Global-scale evaluation of two satellite-based passive microwave soil moisture datasets (SMOS and AMSR-E) with respect to land data assimilation system estimates. Remote Sens Environ, 149: 181–195

Al-Yaari A, Wigneron J P, Kerr Y, Rodriguez-Fernandez N, O'Neill P E, Jackson T J, De Lannoy G J M, Al Bitar A, Mialon A, Richaume P, Walker J P, Mahmoodi A, Yueh S. 2017. Evaluating soil moisture retrievals from ESA's SMOS and NASA's SMAP brightness temperature datasets. Remote Sens Environ, 193: 257–273

Brooks P D, Chorover J, Fan Y, Godsey S E, Maxwell R M, McNamara J P, Tague C. 2015. Hydrological partitioning in the critical zone: Recent advances and opportunities for developing transferable understanding of water cycle dynamics. Water Resour Res, 51: 6973–6987

Brown M E, Escobar V, Moran S, Entekhabi D, O'Neill P E, Njoku E G, Doorn B, Entin J K. 2013. NASA's soil moisture active passive (SMAP) mission and opportunities for applications users. Bull Amer Meteorol Soc, 94: 1125–1128

Chan S K, Bindlish R, O'Neill P, Njoku E, Jackson T, Colliander A, Chen F, Burgin M, Dunbar S, Piepmeier J, Yueh S, Entekhabi D, Cosh M H, Caldwell T, Walker J, Wu X, Berg A, Rowlandson T, Pacheco A, McNairn H, Thibeault M, Martinez-Fernandez J, Gonzalez-Zamora A, Seyfried M, Bosch D, Starks P, Goodrich D, Prueger J, Palecki M, Small E E, Zreda M, Calvet J C, Crow W T, Kerr Y. 2016. Assessment of the SMAP passive soil moisture product. IEEE Trans Geosci Remote Sens, 54: 4994–5007

Chen F, Crow W T, Colliander A, Cosh M H, Jackson T J, Bindlish R, Reichle R H, Chan S K, Bosch D D, Starks P J, Goodrich D C, Seyfried M S. 2017. Application of triple collocation in ground-based validation of soil moisture active/passive (SMAP) Level 2 data products. IEEE J Sel Top Appl Earth Observations Remote Sens, 10: 489–502

Colliander A, Cosh M H, Misra S, Jackson T J, Crow W T, Chan S, Bindlish R, Chae C, Holifield Collins C, Yueh S H. 2017b. Validation and scaling of soil moisture in a semi-arid environment: SMAP validation experiment 2015 (SMAPVEX15). Remote Sens Environ, 196: 101–112

Colliander A, Jackson T J, Bindlish R, Chan S, Das N, Kim S B, Cosh M H, Dunbar R S, Dang L, Pashaian L, Asanuma J, Aida K, Berg A, Rowlandson T, Bosch D, Caldwell T, Caylor K, Goodrich D, al Jassar H, Lopez-Baeza E, Martínez-Fernández J, González-Zamora A, Livingston S, McNairn H, Pacheco A, Moghaddam M, Montzka C, Notarnicola C, Niedrist G, Pellarin T, Prueger J, Pulliainen J, Rautiainen K, Ramos J, Seyfried M, Starks P, Su Z, Zeng Y, van der Velde R, Thibeault M, Dorigo W, Vreugdenhil M, Walker J P, Wu X, Monerris A, O'Neill P E, Entekhabi D, Njoku E G, Yueh S. 2017a. Validation of SMAP surface soil moisture products with core validation sites. Remote Sens Environ, 191: 215–231

Cui H, Jiang L, Du J, Zhao S, Wang G, Lu Z, Wang J. 2017. Evaluation and analysis of AMSR-2, SMOS, and SMAP soil moisture products in the Genhe area of China. J Geophys Res-Atmos, 122: 8650–8666

Das N N, Entekhabi D, Dunbar R S, Njoku E G, Yueh S H. 2016. Uncertainty estimates in the SMAP combined active-passive downscaled brightness temperature. IEEE Trans Geosci Remote Sens, 54: 640–650

De Lannoy G J M, Reichle R H, Peng J, Kerr Y, Castro R, Kim E J, Qing Liu E J. 2015. Converting between SMOS and SMAP level-1 brightness temperature observations over nonfrozen land. IEEE Geosci Remote Sens Lett, 12: 1908–1912

Dente L, Su Z, Wen J. 2012. Validation of SMOS soil moisture products over the Maqu and Twente regions. Sensors, 12: 9965–9986

Ding Y, Baisheng Y E, Zhou W, 1999. Temporal and spatial precipitation distribution in the Heihe Catchment, Northwest China, during the past 40 a (in Chinese). J Glaciol Geocryol, 21: 42–48

Djamai N, Magagi R, Goïta K, Hosseini M, Cosh M H, Berg A, Toth B. 2015. Evaluation of SMOS soil moisture products over the CanEx-SM10 area. J Hydrol, 520: 254–267

Entekhabi D, Njoku E G, O'Neill P E, Kellogg K H, Crow W T, Edelstein W N, Entin J K, Goodman S D, Jackson T J, Johnson J, Kimball J, Piepmeier J R, Koster R D, Martin N, McDonald K C, Moghaddam M, Moran S, Reichle R, Shi J C, Spencer M W, Thurman S W, Tsang L, Van Zyl J. 2010. The soil moisture active passive (SMAP) mission. Proc IEEE, 98: 704–716

Entekhabi D, Yueh S, O'Neill P E, Kellogg K H, Allen A, Bindlish R, Brown M, Chan S, Colliander A, Crow W T, Das N, De Lannoy G, Dunbar R S, Edelstein W N, Entin J K, Escobar V, Goodman S D, Jackson T J, Jai B, Johnson J. 2014. SMAP Handbook. The National Aeronautics and Space Administration

Fernandez-Moran R, Wigneron J P, De Lannoy G, Lopez-Baeza E, Parrens M, Mialon A, Mahmoodi A, Al-Yaari A, Bircher S, Al Bitar A, Richaume P, Kerr Y. 2017. A new calibration of the effective scattering albedo and soil roughness parameters in the SMOS SM retrieval algorithm. Int J Appl Earth Observation Geoinf, 62: 27–38

Frye J D, Mote T L. 2010a. Convection initiation along soil moisture boundaries in the southern Great Plains. Mon Weather Rev, 138: 1140–1151

Frye J D, Mote T L. 2010b. The synergistic relationship between soil moisture and the low-level jet and its role on the prestorm environment in the southern Great Plains. J Appl Meteor Climatol, 49: 775–791

Galantowicz J F, Entekhabi D, Njoku E G. 2000. Estimation of soil-type heterogeneity effects in the retrieval of soil moisture from radio-brightness. IEEE Trans Geosci Remote Sens, 38: 312–315

Gao B, Qin Y, Wang Y, Yang D, Zheng Y. 2016. Modeling ecohydrological processes and spatial patterns in the Upper Heihe Basin in China. Forests, 7: 10

Gherboudj I, Magagi R, Goita K, Berg A A, Toth B, Walker A. 2012. Validation of SMOS data over agricultural and boreal forest areas in Canada. IEEE Trans Geosci Remote Sens, 50: 1623–1635

González-Zamora Á, Sánchez N, Martínez-Fernández J, Gumuzzio Á, Piles M, Olmedo E. 2015. Long-term SMOS soil moisture products: A comprehensive evaluation across scales and methods in the Duero Basin (Spain). Phys Chem Earth Parts A/B/C, 83-84: 123–136

Han X, Franssen H J H, Montzka C, Vereecken H. 2014. Soil moisture and soil properties estimation in the community land model with synthetic brightness temperature observations. Water Resour Res, 50: 6081–6105

Jackson T J, Bindlish R, Cosh M H, Zhao T, Starks P J, Bosch D D, Seyfried M, Moran M S, Goodrich D C, Kerr Y H, Leroux D. 2012. Validation of soil moisture and ocean salinity (SMOS) soil moisture over watershed networks in the U.S.. IEEE Trans Geosci Remote Sens, 50: 1530–1543

Jin M, Zheng X, Jiang T, Li X, Li X J, Zhao K. 2017. Evaluation and improvement of SMOS and SMAP soil moisture products for soils with high organic matter over a forested area in Northeast China. Remote Sens, 9: 387

Kang J, Jin R, Li X, Ma C, Qin J, Zhang Y. 2017. High spatio-temporal resolution mapping of soil moisture by integrating wireless sensor network observations and MODIS apparent thermal inertia in the Babao River Basin, China. Remote Sens Environ, 191: 232–245

Kerr Y H, Waldteufel P, Wigneron J P, Martinuzzi J, Font J, Berger M. 2001. Soil moisture retrieval from space: The Soil Moisture and Ocean Salinity (SMOS) mission. IEEE Trans Geosci Remote Sens, 39: 1729–1735

Kerr Y H, Font J, Martin-Neira M, Mecklenburg S. 2012a. Introduction to the special issue on the ESA's soil moisture and ocean salinity mission (SMOS)—Instrument performance and first results. IEEE Trans Geosci Remote Sens, 50: 1351–1353

Kerr Y H, Al-Yaari A, Rodriguez-Fernandez N, Parrens M, Molero B, Leroux D, Bircher S, Mahmoodi A, Mialon A, Richaume P, Delwart S, Al Bitar A, Pellarin T, Bindlish R, Jackson T J, Rüdiger C, Waldteufel P, Mecklenburg S, Wigneron J P. 2016. Overview of SMOS performance in terms of global soil moisture monitoring after six years in operation. Remote Sens Environ, 180: 40–63

Kerr Y H, Waldteufel P, Richaume P, Wigneron J P, Ferrazzoli P, Mahmoodi A, Al Bitar A, Cabot F, Gruhier C, Juglea S E, Leroux D, Mialon A, Delwart S. 2012b. The SMOS soil moisture retrieval algorithm. IEEE Trans Geosci Remote Sens, 50: 1384–1403

Konings A G, Piles M, Rötzer K, McColl K A, Chan S K, Entekhabi D. 2016. Vegetation optical depth and scattering albedo retrieval using time series of dual-polarized L-band radiometer observations. Remote Sens Environ, 172: 178–189

Koster R D, Dirmeyer P A, Guo Z, Bonan G, Chan E, Cox P, Gordon C T, Kanae S, Kowalczyk E, Lawrence D, Liu P, Lu C H, Malyshev S, McAvaney B, Mitchell K, Mocko D, Oki T, Oleson K, Pitman A, Sud Y C, Taylor C M, Verseghy D, Vasic R, Xue Y, Yamada T, Yamada T. 2004. Regions of strong coupling between soil moisture and precipitation. Science, 305: 1138–1140

Koster R D, Mahanama S P P, Yamada T J, Balsamo G, Berg A A, Boisserie M, Dirmeyer P A, Doblas-Reyes F J, Drewitt G, Gordon C T, Guo Z, Jeong J H, Lawrence D M, Lee W S, Li Z, Luo L, Malyshev S, Merryfield W J, Seneviratne S I, Stanelle T, van den Hurk B J J M, Vitart F, Wood E F. 2010. Contribution of land surface initialization to subseasonal forecast skill: First results from a multi-model experiment. Geophys Res Lett, 37: L02402

Lei F, Huang C, Shen H, Li X. 2014. Improving the estimation of hydrological states in the SWAT model via the ensemble Kalman smoother: Synthetic experiments for the Heihe River Basin in northwest China. Adv Water Resources, 67: 32–45

Leroux D J, Kerr Y H, Richaume P, Fieuzal R. 2013. Spatial distribution and possible sources of SMOS errors at the global scale. Remote Sens Environ, 133: 240–250

Li C, Lu H, Yang K, Han M, Wright J, Chen Y, Yu L, Xu S, Huang X, Gong W. 2018. The evaluation of SMAP enhanced soil moisture products using high-resolution model simulations and *in-situ* observations on the Tibetan Plateau. Remote Sens, 10: 535

Li D, Jin R, Zhou J, Kang J. 2015. Analysis and reduction of the uncertainties in soil moisture estimation with the L-MEB model using EFAST and ensemble retrieval. IEEE Geosci Remote Sens Lett, 12: 1337–1341

Li X, Cheng G, Liu S, Xiao Q, Ma M, Jin R, Che T, Liu Q, Wang W, Qi Y, Wen J, Li H, Zhu G, Guo J, Ran Y, Wang S, Zhu Z, Zhou J, Hu X, Xu Z. 2013. Heihe watershed allied telemetry experimental research (HiWATER): Scientific objectives and experimental design. Bull Amer Meteorol Soc, 94: 1145–1160

Li Z, Xu Z, Shao Q, Yang J. 2009. Parameter estimation and uncertainty analysis of SWAT model in upper reaches of the Heihe river basin. Hydrol Process, 23: 2744–2753

Ma C, Li X, Wei L, Wang W. 2017. Multi-scale validation of SMAP soil moisture products over cold and arid regions in Northwestern China using distributed ground observation data. Remote Sens, 9: 327–341

Ma L, Zhang T, Frauenfeld O W, Qin D. 2006. Verification of ERA-40 and NCEP-1 Reanalysis Temperature Data with Ground-based Measurements in China. American Geophysical Union

Mo T, Choudhury B J, Schmugge T J, Wang J R, Jackson T J. 1982. A model for microwave emission from vegetation-covered fields. J Geophys Res, 87: 11229

O'Neill P, Chan S, Njoku E, Jackson T, Bindlish R. 2015. SMAP Level 2 & 3 Soil Moisture (Passive) Algorithm Theoretical Basis Document. Jet Propulsion Laboratory, Pasadena, CA, USA Revision B

Oliva R, Daganzo E, Kerr Y H, Mecklenburg S, Nieto S, Richaume P, Gruhier C. 2012. SMOS radio frequency interference scenario: Status and actions taken to improve the RFI environment in the 1400–1427-MHz passive band. IEEE Trans Geosci Remote Sens, 50: 1427–1439

O'Neill P, Chan S, Colliander A, Dunbar S, Njoku E, Bindlish R, Chen F, Jackson T, Burgin M, Piepmeier J, Yueh S, Entekhabi D, Cosh M, Caldwell T, Walker J, Wu X, Berg A, Rowlandson T, Pacheco A, McNairn H, Thibeault M, Martínez-Fernández J, González-Zamora Á, Seyfried M, Bosch D, Starks P, Goodrich D, Prueger J, Palecki M, Small E, Zreda M, Calvet J C, Crow W, Kerr Y. 2016. Evaluation of the validated Soil Moisture product from the SMAP radiometer. IGARSS 2016–2016 IEEE International Geoscience and Remote Sensing Symposium IEEE. 125–128

Owe M, de Jeu R, Walker J. 2001. A methodology for surface soil moisture and vegetation optical depth retrieval using the microwave polarization difference index. IEEE Trans Geosci Remote Sens, 39: 1643–1654

Pan M, Cai X, Chaney N W, Entekhabi D, Wood E F. 2016. An initial assessment of SMAP soil moisture retrievals using high-resolution model simulations and *in situ* observations. Geophys Res Lett, 43: 9662–9668

Panciera R, Walker J P, Kalma J D, Kim E J, Saleh K, Wigneron J P. 2009. Evaluation of the SMOS L-MEB passive microwave soil moisture retrieval algorithm. Remote Sens Environ, 113: 435–444

Parrens M, Zakharova E, Lafont S, Calvet J C, Kerr Y, Wagner W, Wigneron J P. 2012. Comparing soil moisture retrievals from SMOS and ASCAT over France. Hydrol Earth Syst Sci, 16: 423–440

Pellarin T, Mialon A, Biron R, Coulaud C, Gibon F, Kerr Y, Lafaysse M, Mercier B, Morin S, Redor I, Schwank M, Völksch I. 2016. Three years of L-band brightness temperature measurements in a mountainous area: Topography, vegetation and snowmelt issues. Remote Sens Environ, 180: 85–98

Polcher J, Piles M, Gelati E, Barella-Ortiz A, Tello M. 2016. Comparing surface-soil moisture from the SMOS mission and the ORCHIDEE land-surface model over the Iberian Peninsula. Remote Sens Environ, 174: 69–81

Reichle R, Koster R, De Lannoy G, Crow W, Kimball J. 2014. Algorithm Theoretical Basis Document Level 4 Surface and Root Zone Soil Moisture (L4_SM) Data Product. NASA. 3

Richter D B, Mobley M L. 2009. Monitoring Earth's Critical Zone. Science, 326: 1067–1068
Ridler M E, Madsen H, Stisen S, Bircher S, Fensholt R. 2014. Assimilation of SMOS-derived soil moisture in a fully integrated hydrological and soil-vegetation-atmosphere transfer model in Western Denmark. Water Resour Res, 50: 8962–8981
Rötzer K, Montzka C, Bogena H, Wagner W, Kerr Y H, Kidd R, Vereecken H. 2014. Catchment scale validation of SMOS and ASCAT soil moisture products using hydrological modeling and temporal stability analysis. J Hydrol, 519: 934–946
Srivastava P K, Han D, Rico Ramirez M A, Islam T. 2013. Appraisal of SMOS soil moisture at a catchment scale in a temperate maritime climate. J Hydrol, 498: 292–304
Taylor C M. 2015. Detecting soil moisture impacts on convective initiation in Europe. Geophys Res Lett, 42: 4631–4638
Vereecken H, Huisman J A, Pachepsky Y, Montzka C, van der Kruk J, Bogena H, Weihermüller L, Herbst M, Martinez G, Vanderborght J. 2014. On the spatio-temporal dynamics of soil moisture at the field scale. J Hydrol, 516: 76–96
Vreugdenhil M, Dorigo W, Broer M, Haas P, Eder A, Hogan P, Bloeschl G, Wagner W, 2013. Towards a high-density soil moisture network for the validation of SMAP in Petzenkirchen, Austria. IGARSS 2013–2013 IEEE International Geoscience and Remote Sensing Symposium IEEE. 1865–1868, doi: 10.1109/IGARSS.2013.6723166
Wang C, Zhao C Y. 2013. A study of the spatio-temporal distribution of precipitation in upper reaches of Heihe River of China using TRMM data (in Chinese). J Nat Resour, 28: 862–872
Wigneron J P, Kerr Y, Waldteufel P, Saleh K, Escorihuela M J, Richaume P, Ferrazzoli P, de Rosnay P, Gurney R, Calvet J C, Grant J P, Guglielmetti M, Hornbuckle B, Mätzler C, Pellarin T, Schwank M. 2007. L-band Microwave Emission of the Biosphere (L-MEB) Model: Description and calibration against experimental data sets over crop fields. Remote Sens Environ, 107: 639–655
Wigneron J P, Schwank M, Baeza E L, Kerr Y, Novello N, Millan C, Moisy C, Richaume P, Mialon A, Al Bitar A, Cabot F, Lawrence H, Guyon D, Calvet J C, Grant J P, Casal T, de Rosnay P, Saleh K, Mahmoodi A, Delwart S, Mecklenburg S. 2012. First evaluation of the simultaneous SMOS and ELBARA-II observations in the Mediterranean region. Remote Sens Environ, 124: 26–37
Wu Q, Liu H, Wang L, Deng C. 2016. Evaluation of AMSR2 soil moisture products over the contiguous United States using *in situ* data from the international soil moisture network. Int J Appl Earth Observation Geoinf, 45: 187–199
Yang L, Sun G, Zhi L, Zhao J. 2018. Negative soil moisture-precipitation feedback in dry and wet regions. Sci Rep, 8: 4026
Zhang L, He C, Li J, Wang Y, Wang Z. 2017b. Comparison of IDW and physically based IDEW method in hydrological modelling for a large mountainous watershed, Northwest China. River Res Applic, 33: 912–924
Zhang L, He C, Zhang M. 2017a. Multi-scale evaluation of the SMAP product using sparse *in-situ* network over a high mountainous watershed, Northwest China. Remote Sens, 9: 1111–1132
Zhao L, Yang K, Qin J, Chen Y, Tang W, Lu H, Yang Z L. 2014. The scale-dependence of SMOS soil moisture accuracy and its improvement through land data assimilation in the central Tibetan Plateau. Remote Sens Environ, 152: 345–355
Zhao T, Shi J, Bindlish R, Jackson T, Cosh M, Jiang L, Zhang Z, Lan H. 2015. Parametric exponentially correlated surface emission model for L-band passive microwave soil moisture retrieval. Phys Chem Earth Parts A/B/C, 83-84: 65–74

(Responsible editor: Qiuhong TANG)